Solar Water Splitting

Deutsche Ausgabe: DOI: 10.1002/ange.201605924
Internationale Ausgabe: DOI: 10.1002/anie.201605924

Highly Conformal Deposition of an Ultrathin FeOOH Layer on a Hematite Nanostructure for Efficient Solar Water Splitting

*Jae Young Kim, Duck Hyun Youn, Kyoungwoong Kang, and Jae Sung Lee**

Abstract: *An ultrathin (ca. 2 nm) amorphous FeOOH overlayer was deposited conformally on a hematite nanostructure by a simple solution-based precipitation method, to generate an oxygen evolution cocatalyst for efficient solar water splitting. This uniform and highly conformal coating of the ultrathin metal oxyhydroxide is rare and is distinguished from the layers prepared by other conventional methods. With the FeOOH overlayer as the cocatalyst, the water oxidation photocurrent of hematite increased by a factor of approximately two and the onset potential shifted in the cathodic direction by 0.12 V under 1 sun illumination. The enhanced performance was attributed to the improved water oxidation kinetics and the passivation of the surface states of the hematite.*

Photoelectrochemical (PEC) water oxidation under sunlight has been actively investigated as an important step for eco-friendly hydrogen production from water splitting and artificial photosynthesis from CO_2 reduction.[1–3] Under illumination photo-excited electron–hole pairs are generated in semiconductors; holes oxidize water according to Equation 1.

$$2\,H_2O(l) + h\nu \rightarrow O_2(g) + 4\,H^+ + 4\,e^- \quad (1)$$

Hematite (α-Fe_2O_3) is one of the most popular photoanode materials for this application because of its desirable band gap for ample visible-light absorption (ca. 2.1 eV), ready availability, and robustness in alkaline electrolytes.[2,4] Hematite photoanodes are often fabricated into a nanostructured thin film to address its short hole diffusion length (2–4 nm) and minimize electron–hole recombination in the bulk.[4–6] Additionally, introduction of a catalytic overlayer to the surface of the semiconductor is a popular strategy to promote charge separation at the surface.[7–9] The overlayer generally passivates the surface states and/or improves oxygen evolution kinetics.[7] Noble metal oxides (for example, IrO_2 and RuO_2) are representative traditional materials applied as oxygen evolution cocatalysts,[10] and some amorphous phosphates, borates, and carbonates (for example, Co-Pi, Ni-Bi, and Co-Ci) have also been studied in recent years.[4,11–14] Amorphous oxyhydroxides have been developed recently as highly efficient cocatalyst layers for some semiconductor thin film photoanodes.[15–17] For example, a $BiVO_4$-based photoanode with FeOOH/NiOOH dual overlayers showed record-breaking photocurrents for PEC water oxidation under sunlight.[16]

The most common method to deposit an oxyhydroxide overlayer onto a semiconductor is (photo-assisted) electrodeposition.[15–17] The method usually forms thick (0.1–10 μm) and non-uniform layers independent of the morphology of the underlying substrate surface.[16] On the other hand, the present study employs a simple solution-based precipitation method, in which the hematite thin film is simply immersed in a hot aqueous solution containing precursor ions to let amorphous FeOOH grow on the hematite surface.[18] To our best knowledge, it is the first attempt to apply the precipitation method to deposition of an amorphous oxyhydroxide layer on a semiconductor thin film as a cocatalyst for water oxidation. To our surprise, the precipitation method produced a highly conformal and ultrathin (1–3 nm) FeOOH overlayer, which reflected the original morphology of the Fe_2O_3 substrate well. The conformal coating could not be obtained by conventional deposition techniques, such as electrodeposition.

Such conformal deposition is possible by controlling the interfacial energies within the system.[18] Under a low pH and high ionic strength environment, the interfacial energy between the overlayer and the substrate (herein, amorphous FeOOH and α-Fe_2O_3 nanostructure) is smaller than the interfacial energy between the overlayer and the solution. Therefore, nuclei will appear on the entire substrate and will result in conformal deposition. By this method, we can obtain a robust thin layer with better adherence and mechanical stability—unlike some indirect deposition techniques.[4,8,18] Additionally, the layer may be more effective for passivation of the substrate because of its near perfect coverage—even on complicated substrate morphologies. Another advantage of the precipitation method is that the thickness is controllable in approximately nanometer scale so that the layer is transparent enough to be applied to tandem PEC devices, where the second light absorber utilizes the light transmitted through the first absorber to generate electron–hole pairs.[19]

Thus, an ultrathin amorphous FeOOH layer of optimized uniform thickness of about 2 nm was formed on a hematite nanostructure (FeOOH/Fe_2O_3) by the precipitation method. The FeOOH/Fe_2O_3 was fabricated into a photoanode, showing much improved performance for PEC water oxidation because of the effects of surface passivation and/or improved oxygen evolution kinetics. We expect the current simple method could be generally applied to the deposition of conformal thin passivating films instead of expensive physical/chemical vapor-deposition techniques.[20,21] The method

[*] Dr. J. Y. Kim, Dr. D. H. Youn, K. Kang, Prof. J. S. Lee
School of Energy and Chemical Engineering
Ulsan National Institute of Science and Technology (UNIST)
50 UNIST-gil, Ulsan 44919 (Republic of Korea)
E-mail: jlee1234@unist.ac.kr

Supporting information for this article can be found under: http://dx.doi.org/10.1002/anie.201605924.

could also be applied equally well to other substrates, such as monocrystalline Al_2O_3, polycrystalline ITO or FTO glasses, Si/SiO_2 wafers, and nanostructured ZnO thin films.[22–24]

The hematite electrode was synthesized by a simple solution-based method to grow β-FeOOH nanorods on $F:SnO_2$ coated glass (FTO), followed by high temperature annealing at 800 °C for 20 min to obtain a red–orange Fe_2O_3 film, as described previously.[4,8,18] Subsequently, the FeOOH overlayer was deposited by immersing Fe_2O_3/FTO into an aqueous solution of $FeCl_3 \cdot 6H_2O$ (0.15 M) and $NaNO_3$ (1 M) at 100 °C for 5 min. In the SEM images (Figure 1), both bare

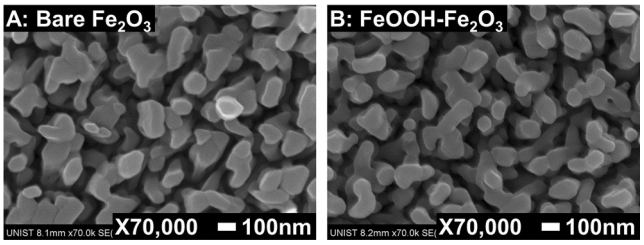

Figure 1. SEM images for the A) bare Fe_2O_3 and B) FeOOH/Fe_2O_3 thin films. No morphological difference is an indication of highly conformal coating of Fe_2O_3 by an ultrathin FeOOH layer.

Fe_2O_3 and FeOOH/Fe_2O_3 exhibited an identical surface morphology of wormlike particles, which were 70–100 nm in size. This indicates a highly conformal coating of Fe_2O_3 particles by ultra-thin layers of FeOOH. As shown in Figure S1 (Supporting Information), they present the same X-ray diffraction patterns as hematite (α-Fe_2O_3), with a dominant (110) peak at $2\theta = 35.8$ indicating preferential orientation of hematite crystals in the [110] direction.[4,25] The FeOOH overlayer does not show any significant diffraction since it is thin and amorphous.

The HRTEM images in Figure 2 show clear lattice fringes corresponding to (110) planes of the monocrystalline Fe_2O_3. A very thin amorphous FeOOH layer is observed in Figure 2 B. The thickness of the layer is approximately 2 nm and it is highly uniform, as might be expected of a typical conformal coating. It should be mentioned that the thickness of the overlayer is much thinner (by a factor of ca. 1000) than that of the films obtained by conventional electrodeposition. A Fast Fourier Transfer (FFT) pattern obtained from the crystalline Fe_2O_3 shows a clear pattern of dots, while that obtained from the amorphous overlayer is blurry. Additional TEM images at various positions (Supporting Information, Figure S2) confirm that the entire surface of the Fe_2O_3 nanostructure is wrapped in thin amorphous layers. The Fe 2p XPS spectra in Figure S3 (Supporting Information) show that both films contain only Fe^{3+} species. But O 1s spectra show that FeOOH/Fe_2O_3 has an OH peak of a higher intensity than that for the bare Fe_2O_3, which is consistent with the reports on FeOOH in the literature (for which the OH peak makes up about 45 % of the total O 1s peak area).[26,27] The results identify that the thin amorphous layer is FeOOH. The analyses clearly demonstrate that highly crystalline hematite is coated by an ultrathin and amorphous FeOOH

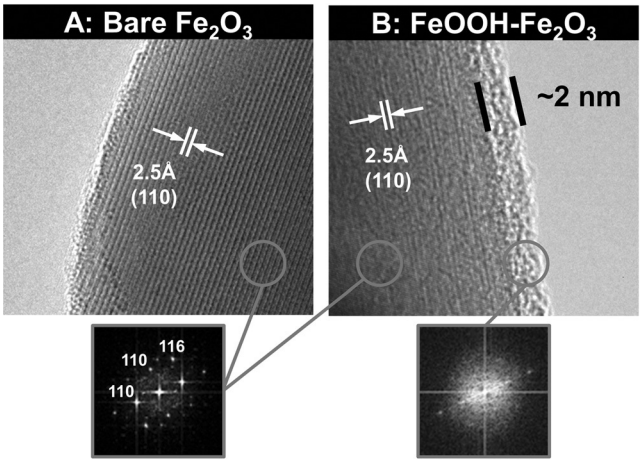

Figure 2. HRTEM images for the A) bare Fe_2O_3 and B) FeOOH/Fe_2O_3 thin films. Both films contain monocrystalline Fe_2O_3 with clear lattice fringes, but only (B) contains the amorphous FeOOH layer with a thickness of about 2 nm. The bottom images are FFT patterns showing clear dots for the crystalline Fe_2O_3 and a blurry pattern for the amorphous FeOOH.

layer. Usually, a highly conformal coating can only be obtained by special chemical vapor or atomic layer deposition, and not by common solution-based deposition techniques.

The bare Fe_2O_3 and FeOOH/Fe_2O_3 thin films were fabricated into photoanodes for water oxidation under 1 sun irradiation. PEC measurements were made in a typical three-electrode cell with photoanodes, platinum mesh, and Ag/AgCl as working, counter, and reference electrodes, respectively, in an aqueous NaOH (1 M, pH 13.6) electrolyte. The deposition time of the FeOOH overlayer was optimized with respect to water oxidation photocurrents, and the optimum time required for formation of an approximately 2 nm FeOOH layer was 5 min (Supporting Information, Figure S4). A longer deposition time gave a thicker layer with a reduced water oxidation performance, which is probably due to the interference of light absorption and an elongated hole diffusion path from Fe_2O_3 to the electrolyte.

The current density–potential (J–V) curves are exhibited in Figure 3. When the FeOOH overlayer is deposited on Fe_2O_3, the water oxidation photocurrent increases by a factor of about two (0.612→1.21 mA cm^{-2} at 1.23 V_{RHE}) and its current onset potential shifts in the cathodic direction by 0.12 V (0.77→0.65 V_{RHE}). The changes are typical of an efficient cocatalyst that improves the PEC water oxidation kinetics of the photoanode. Table S1 (Supporting Information) compares several reported oxyhydroxide cocatalysts on α-Fe_2O_3 or $BiVO_4$ photoelectrodes for solar water oxidation.[16,28–32] As the present study is the first example of a FeOOH/α-Fe_2O_3 system, a comparison was made with some NiOOH/α-Fe_2O_3 and FeOOH/$BiVO_4$ systems. While the previous reported systems record 23–47 % photocurrent increases (ΔJ_{ph}) for Fe_2O_3 electrodes, the present study records a 97 % increase, along with a comparable onset potential shift (ΔV_{Onset}). Thus the current solution-based precipitation method for deposition of an overlayer of

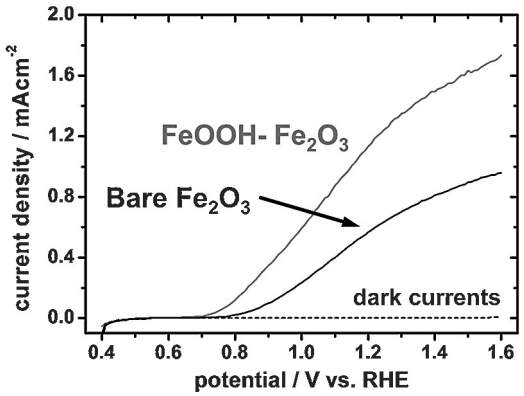

Figure 3. Current density–potential curves recorded at pH 13.6 (1 M NaOH) under 1 sun simulated solar light irradiation.

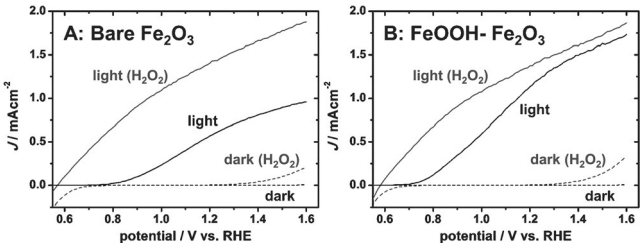

Figure 4. *J–V* curves for the A) bare Fe_2O_3 and B) FeOOH/Fe_2O_3 photoanodes. For photo-oxidation of the hole scavenger, a NaOH (1 M) electrolyte containing H_2O_2 (0.5 M) was used under 1 sun irradiation.

oxygen evolution cocatalyst is demonstrated to be highly effective for fabrication of efficient photoanodes for solar water oxidation. This is probably due to the near perfect conformal coating of ultrathin FeOOH layers that effectively passivates the semiconductor surface. By comparison, electrodeposition methods seem more suited to $BiVO_4$ systems, according to their high ΔJ_{ph} (>200 %).[16,28,29] A control FeOOH/Fe_2O_3 sample was prepared using the conventional photo-assisted electrodeposition method and its *J–V* curve is presented in Figure S5 (Supporting Information). The photocurrent at 1.23 V_{RHE} of the control sample only increased by 36 %. The improvement is much lower compared with FeOOH–Fe_2O_3 prepared by the precipitation method (97 %), but it is consistent with the values obtained from other oxyhydroxide/Fe_2O_3 systems (23–47 %; Supporting Information, Table S1).

The stability of the photoanode was fairly good, as shown in Figure S6 (Supporting Information), where photocurrent at 1.23 V_{RHE} decreased from its initial value by less than 3 % in 150 min. The TEM image after the stability test (Supporting Information, Figure S7) shows that the amorphous overlayer stayed on the surface of the hematite nanostructure well. The products of PEC water splitting were analyzed by gas chromatography during the stability test. As shown in Figure S8 (Supporting Information), H_2 and O_2 were detected by GC in a stoichiometric 2:1 ratio and their amounts increased linearly with time. Faradaic efficiency (F.E.) was also calculated; 96–99 % for H_2 and 92–95 % for O_2. This demonstrates that the current is primarily generated from water splitting with negligible parasitic effects (corrosion for example).

The improved water oxidation kinetics by FeOOH deposition usually originate from increased charge separation efficiency on the surface of the photoanode. To prove this conjecture, we studied the photo-oxidation of a well-known hole scavenger, H_2O_2. Since the surface charge separation of H_2O_2 oxidation is essentially complete because of its high reactivity, comparison of its photocurrent (J^{H2O2}) with that of water oxidation (J^{H2O}) gives the extent of surface charge separation.[33,34] Figure 4 compares *J–V* curves for photo-oxidation of water with and without H_2O_2 (0.5 M) as a hole scavenger. The gap between the two *J–V* curves of water and H_2O_2 indicate the inefficiency of surface charge separation. As the catalytic FeOOH overlayer is introduced, the gap between J^{H2O} and J^{H2O2} is greatly reduced, indicating improved surface charge separation on FeOOH/Fe_2O_3.

For a more quantitative analysis, the surface charge separation efficiency (η_{surf}) was determined with Equation 2.

$$\eta_{surf} = J^{H2O}/J^{H2O2} \quad (2)$$

The calculated efficiencies presented in Figure S9 (Supporting Information) indicate that the η_{surf} values for the FeOOH/Fe_2O_3 photoanode are about two times higher than those for bare Fe_2O_3 over the entire potential range. The results demonstrate that the improved photocurrent generation and onset potential shift for FeOOH/Fe_2O_3 originates from the improved surface charge separation efficiency. It is also noteworthy that, although our method forms ultrathin layers of only a few nanometer thickness, the extent of the effect is comparable with, or better than, those of thick catalytic overlayers of a few micrometers prepared by electrodeposition techniques.

For further electrochemical characterization, Mott–Schottky analysis was performed (Supporting Information, Figure S10). Two photoanodes do not show any significant difference in the charge carrier density derived from the slope of the Mott–Schottky plot, but the flat-band potential derived from the intercept of the *x*-axis shows a shift in the cathodic direction by 0.12 V. This shift is also consistent with the shift in the current onset potential in the *J–V* curves in Figure 3. One possible explanation for the shifted flat-band potential is the passivation of surface states by the overlayers. The surface states cause a potential drop within the Helmholtz layer but this can be minimized with surface passivation.[35] The conformal FeOOH overlayer may passivate the surface of the nanostructured Fe_2O_3 more effectively by providing a larger contact area between the Fe_2O_3 and passivation layer, with less exposure of the bare Fe_2O_3 surface than that for non-uniform layers formed by the electrodeposition method.

The electrochemical impedance spectra (Nyquist plots) are displayed in Figure S11 (Supporting Information) at 1.23 V_{RHE} under 1 sun irradiation. The impedance spectra were fitted to an equivalent circuit, as shown.[36,37] R2 of the circuit is assigned to the resistance arising from the water oxidation reaction at the interface between the photoanode and the electrolyte. It is reduced after the overlayer

deposition (538→373 Ω), suggesting that water oxidation proceeds much more easily on the surface of the FeOOH/Fe_2O_3 photoanode than on bare Fe_2O_3. R1 (charge transfer resistance in the bulk Fe_2O_3) is also reduced, possibly because of the enhanced charge separation in the part close to the passivated surface.

The absorption of sunlight by oxygen evolution co-catalysts is another potential problem if the photoanodes form a tandem PEC device with multiple light absorbers.[19] Figure S12 (Supporting Information) shows that light harvesting efficiency (η_{LH}) of bare Fe_2O_3 and FeOOH/Fe_2O_3 is identical; this is calculated from the UV/Vis absorbance and the equation $\eta_{LH} = 1—10^{-A}$ (A = absorbance). The amorphous FeOOH overlayer prepared by the current method is transparent enough to fabricate a tandem device without any light loss. It is a significant advantage of the current method. We can control the thickness of the layer more precisely (approximately nanometer scale) than electrodeposition techniques allow, by varying the deposition time.

In conclusion, for the first time a highly conformal coating of ultrathin (ca. 2 nm) amorphous FeOOH overlayer on a hematite nanostructure was successfully carried out by a simple precipitation method. The resultant material was applied as a cocatalyst for efficient solar water splitting. The FeOOH overlayer was surprisingly thin (ca. 2 nm) and uniform, and the thickness was only about 1/1000 of the non-uniform layers obtained by conventional electrodeposition. When the FeOOH overlayer is applied, the water oxidation photocurrent increases by a factor of about two, and its onset potential shifts in the cathodic direction by 0.12 V, exhibiting the typical beneficial effects of efficient cocatalysts for PEC water splitting. The enhanced performance is attributed to the improved water oxidation kinetics and the passivation effect of the surface states present on the hematite substrate. The current, simple and low cost, solution-phase method may be generically applied to the deposition of nanoscale passivating thin layers, as opposed to expensive conventional physical/chemical vapor-deposition techniques.

Experimental Section

The hematite electrodes were prepared by a simple solution-based method and high temperature annealing at 800 °C.[34] The starting material (β-FeOOH) was grown on F:SnO_2 coated glass (FTO) purchased from Pilkington Inc. (TEC8) at 100 °C in an aqueous solution of $FeCl_3 \cdot 6H_2O$ (0.15 M) and $NaNO_3$ (1 M). After drying at ambient temperature overnight, the yellow thin film was annealed at 800 °C for just 20 min using a conventional thermal furnace to obtain a red–orange bare Fe_2O_3 thin film on FTO. For the deposition of the FeOOH overlayer, the Fe_2O_3 thin film was immersed in a hot (100 °C) aqueous solution containing $FeCl_3 \cdot 6H_2O$ (0.15 M) and $NaNO_3$ (1 M) for various time durations. The FeOOH/Fe_2O_3 thin film was washed with an excess volume of distilled water and dried at ambient temperature overnight. The control sample was prepared using photo-assisted electrodeposition at 0.45 V_{RHE} with the bare Fe_2O_3 as a working electrode in a $FeCl_2$ (0.1 M) solution under 1 sun irradiation.[28–32] Electrical contact was made with silver paste and copper wire.

Solar water oxidation was performed in a three-electrode cell with the photoanode as a working electrode, a platinum mesh as a counter electrode and Ag/AgCl as a reference electrode in NaOH (1 M, pH 13.6) electrolyte. Photocurrent–potential curves and electrochemical impedance spectra were recorded under simulated solar light generated by a solar simulator (91170, Oriel) with an air mass 1.5 G filter. Light intensity of the solar simulator was calibrated to 1 sun (100 mW cm^{-2}) using a reference cell certified by the National Renewable Energy Laboratories (U.S.). All electrochemical measurements were performed using a potentiostat (IviumStat, Ivium Technologies). Electrochemical impedance spectra (EIS) were recorded at DC potential 1.23 V_{RHE} and an AC potential frequency range of 100000–0.1 Hz with an amplitude of 10 mV. Software (ZView, Scribner Associates) was used for fitting of the experimental EIS data to an equivalent circuit model. Water splitting products (H_2 and O_2) were analyzed by gas chromatography (GC), with Ar as a carrier gas, using a closed circulation system.[4]

To characterize the hematite thin films, X-ray diffraction (PW3040/60 X′pert PRO, PANalytical with $Cu_{K\alpha}$ ($\lambda = 1.54056$ Å) radiation), HR-TEM (JEM-2200FS, JEOL with Cs-corrector), and HR-SEM (JSM-7401F, JEOL) were used. For HR-TEM, the powder was prepared by grinding the hematite thin film surface with sandpaper and dispersing it in ethanol.

Acknowledgements

This work was supported by Brain Korea Plus Program of Ministry of Education, Korean Center for Artificial Photosynthesis (NRF-2011-C1AAA0001-2011-0030278), Climate Change Response project (2015M1A2A2074663), the Basic Science Grant (NRF-2015R1A2A1A10054346) funded by MSIP, and Project No. 10050509 funded by MOTIE of the Republic of Korea.

Keywords: amorphous FeOOH overlayer · hematite · oxygen evolution cocatalysts · solar water splitting · surface passivation

How to cite: *Angew. Chem. Int. Ed.* **2016**, *55*, 10854–10858
Angew. Chem. **2016**, *128*, 11012–11016

[1] A. Fujishima, K. Honda, *Nature* **1972**, *238*, 37–38.
[2] K. Sivula, F. Le Formal, M. Grätzel, *ChemSusChem* **2011**, *4*, 432–449.
[3] Y. Tachibana, L. Vayssieres, J. R. Durrant, *Nat. Photonics* **2012**, *6*, 511–518.
[4] J. Y. Kim, G. Magesh, D. H. Youn, J.-W. Jang, J. Kubota, K. Domen, J. S. Lee, *Sci. Rep.* **2013**, *3*, 2681.
[5] I. Cesar, A. Kay, J. A. G. Martinez, M. Grätzel, *J. Am. Chem. Soc.* **2006**, *128*, 4582–4583.
[6] K. Sivula, R. Zboril, F. Le Formal, R. Robert, A. Weidenkaff, J. Tucek, J. Frydrich, M. Grätzel, *J. Am. Chem. Soc.* **2010**, *132*, 7436–7444.
[7] L. Steier, I. Herraiz-Cardona, S. Gimenez, F. Fabregat-Santiago, J. Bisquert, S. D. Tilley, M. Grätzel, *Adv. Funct. Mater.* **2014**, *24*, 7681–7688.
[8] J. Y. Kim, J.-W. Jang, D. H. Youn, G. Magesh, J. S. Lee, *Adv. Energy Mater.* **2014**, *4*, 1400476.
[9] M. G. Ahmed, I. E. Kretschmer, T. A. Kandiel, A. Y. Ahmed, F. A. Rashwan, D. W. Bahnemann, *ACS Appl. Mater. Interfaces* **2015**, *7*, 24053–24062.
[10] R. Hutchings, K. Müller, R. Kötz, S. Stucki, *J. Mater. Sci.* **1984**, *19*, 3987–3994.
[11] D. K. Zhong, M. Cornuz, K. Sivula, M. Grätzel, D. R. Gamelin, *Energy Environ. Sci.* **2011**, *4*, 1759–1764.
[12] A. J. Esswein, Y. Surendranath, S. Y. Reece, D. G. Nocera, *Energy Environ. Sci.* **2011**, *4*, 499–504.

[13] J. H. Kim, G. Magesh, H. J. Kang, M. Banu, J. H. Kim, J. Lee, J. S. Lee, *Nano Energy* **2015**, *15*, 153 – 163.
[14] J. H. Kim, Y. Jo, J. W. Jang, H. J. Kang, Y. H. Lee, D. S. Kim, Y. Jun, J. S. Lee, *ACS Nano* **2015**, *9*, 11820 – 11829.
[15] W. D. Chemelewski, H.-C. Lee, J.-F. Lin, A. J. Bard, C. B. Mullins, *J. Am. Chem. Soc.* **2014**, *136*, 2843 – 2850.
[16] T. W. Kim, K.-S. Choi, *Science* **2014**, *343*, 990 – 994.
[17] L. Trotochaud, S. L. Young, J. K. Ranney, S. W. Boettcher, *J. Am. Chem. Soc.* **2014**, *136*, 6744 – 6753.
[18] L. Vayssieres, N. Beermann, S.-E. Lindquist, A. Hagfeldt, *Chem. Mater.* **2001**, *13*, 233 – 235.
[19] C. G. Morales-Guio, M. T. Mayer, A. Yella, S. D. Tilley, M. Grätzel, X. Hu, *J. Am. Chem. Soc.* **2015**, *137*, 9927 – 9936.
[20] F. Le Formal, N. Tetreault, M. Cornuz, T. Moehl, M. Grätzel, K. Sivula, *Chem. Sci.* **2011**, *2*, 737 – 743.
[21] Y. Lin, Y. Xu, M. T. Mayer, Z. I. Simpson, G. McMahon, D. Wang, *J. Am. Chem. Soc.* **2012**, *134*, 5508 – 5511.
[22] L. Vayssieres, *Adv. Mater.* **2003**, *15*, 464 – 466.
[23] L. Vayssieres, K. Keis, A. Hagfeldt, S.-E. Lindquist, *Chem. Mater.* **2001**, *13*, 4395 – 4398.
[24] L. Vayssieres, K. Keis, S.-E. Lindquist, A. Hagfeldt, *J. Phys. Chem. B* **2001**, *105*, 3350 – 3352.
[25] M. Cornuz, M. Grätzel, K. Sivula, *Chem. Vap. Deposition* **2010**, *16*, 291 – 295.
[26] I. D. Welsh, P. M. A. Sherwood, *Phys. Rev. B* **1989**, *40*, 6386 – 6392.
[27] N. S. McIntyre, D. G. Zetaruk, *Anal. Chem.* **1977**, *49*, 1521 – 1529.
[28] Y. Park, D. Kang, K.-S. Choi, *Phys. Chem. Chem. Phys.* **2014**, *16*, 1238 – 1246.
[29] J. A. Seabold, K. Zhu, N. R. Neale, *Phys. Chem. Chem. Phys.* **2014**, *16*, 1121 – 1131.
[30] F. Malara, A. Minguzzi, M. Marelli, S. Morandi, R. Psaro, V. Dal Santo, A. Naldoni, *ACS Catal.* **2015**, *5*, 5292 – 5300.
[31] A. G. Tamirat, W.-N. Su, A. A. Dubale, H.-M. Chen, B.-J. Hwang, *J. Mater. Chem. A* **2015**, *3*, 5949 – 5961.
[32] Z. Wang, G. Liu, C. Ding, Z. Chen, F. Zhang, J. Shi, C. Li, *J. Phys. Chem. C* **2015**, *119*, 19607 – 19612.
[33] H. Dotan, K. Sivula, M. Grätzel, A. Rothschild, S. C. Warren, *Energy Environ. Sci.* **2011**, *4*, 958 – 964.
[34] J. Y. Kim, D. H. Youn, J. H. Kim, H. G. Kim, J. S. Lee, *ACS Appl. Mater. Interfaces* **2015**, *7*, 14123 – 14129.
[35] C. Du, X. Yang, M. T. Mayer, H. Hoyt, J. Xie, G. McMahon, G. Bischoping, D. Wang, *Angew. Chem. Int. Ed.* **2013**, *52*, 12692 – 12695; *Angew. Chem.* **2013**, *125*, 12924 – 12927.
[36] B. Klahr, S. Gimenez, F. Fabregat-Santiago, T. Hamann, J. Bisquert, *J. Am. Chem. Soc.* **2012**, *134*, 4294 – 4302.
[37] B. Klahr, S. Gimenez, F. Fabregat-Santiago, J. Bisquert, T. W. Hamann, *J. Am. Chem. Soc.* **2012**, *134*, 16693 – 16700.

Received: June 19, 2016
Published online: August 4, 2016

